

Article

# Rheological and Electrochemical Properties of Biodegradable Chia Mucilage Gel Electrolyte Applied to Supercapacitor

Inkyum Kim <sup>1</sup>, Su Thiri San <sup>1</sup>, Avinash C. Mendhe <sup>2</sup>, Suprimkumar D. Dhas <sup>2</sup>, Seung-Bae Jeon <sup>3,\*</sup> and Daewon Kim <sup>2,\*</sup> 

<sup>1</sup> Department of Electronics and Information Convergence Engineering, Kyung Hee University, 1732 Deogyeong-daero, Giheung-gu, Yongin 17104, Republic of Korea; inkyum.kim@khu.ac.kr

<sup>2</sup> Department of Electronic Engineering, Kyung Hee University, 1732 Deogyeong-daero, Giheung-gu, Yongin 17104, Republic of Korea; avinashm2893@khu.ac.kr

<sup>3</sup> Department of Electronic Engineering, Hanbat National University, 125 Dongseo-daero, Yuseong-gu, Daejeon 34158, Republic of Korea

\* Correspondence: sbjeon@hanbat.ac.kr (S.-B.J.); daewon@khu.ac.kr (D.K.)

**Abstract:** The flexible energy storage device of high demand in wearable and portable electronics. Flexible supercapacitors have benefits over flexible batteries, and their development relies on the use of flexible components. Gel polymer electrolytes have the merits of liquid and solid electrolytes and are used in flexible devices. In this study, a gel derived from chia seed was used as a flexible electrolyte material, and its rheological, thermal, and electrochemical properties were investigated. High thermal stability and shear thinning behavior were observed via the electrolyte state of the chia mucilage gel. Compared to the conventional salt electrolyte, the chia mucilage gel electrolyte-based supercapacitor exhibited a more rectangular cyclic voltammetry (CV) curve, longer discharging time in galvanostatic charge–discharge (GCD) analysis, and low charge transfer resistance in electrochemical impedance spectroscopy (EIS). The maximum specific capacitance of  $7.77 \text{ F g}^{-1}$  and power density of  $287.7 \text{ W kg}^{-1}$  were measured, and stable capacitance retention of 94% was achieved after 10,000 cycles of charge/discharge with harsh input conditions. The biodegradability was also confirmed by the degraded mucilage film in soil after 30 days. The plant-driven chia mucilage gel electrolyte can facilitate the realization of flexible supercapacitors for the energy storage devices of the future.

**Keywords:** gel electrolyte; chia seed mucilage; supercapacitor; biodegradability; rheology



**Citation:** Kim, I.; San, S.T.; Mendhe, A.C.; Dhas, S.D.; Jeon, S.-B.; Kim, D. Rheological and Electrochemical Properties of Biodegradable Chia Mucilage Gel Electrolyte Applied to Supercapacitor. *Batteries* **2023**, *9*, 512. <https://doi.org/10.3390/batteries9100512>

Academic Editor: Pascal Venet

Received: 22 September 2023

Revised: 11 October 2023

Accepted: 13 October 2023

Published: 17 October 2023



**Copyright:** © 2023 by the authors. Licensee MDPI, Basel, Switzerland. This article is an open access article distributed under the terms and conditions of the Creative Commons Attribution (CC BY) license (<https://creativecommons.org/licenses/by/4.0/>).

## 1. Introduction

Flexible wearable electronic devices are becoming more popular as they offer convenience, comfort, and lightness for various applications such as flexible sensors and artificial electronic skin [1–7]. However, these devices also need flexible wearable power sources that can provide reliable and sustainable electrical energy storage with high safety, mechanical strength, and electrochemical performance [8–11]. Flexible electrochemical energy storage devices are a promising option, but they also face some challenges such as thermal runaway and low energy density [12]. Therefore, it is important to explore new ways to improve the preparation process and performance of these devices.

Flexible supercapacitors are a type of flexible energy storage devices that use electrical double layer formation or surface Faradaic reaction of nanomaterials to store energy [13,14]. They have many benefits over flexible batteries, such as high power density, fast charging and discharging, wide temperature range, high efficiency, long cycle life, and higher security. The main components of flexible supercapacitors are flexible electrode materials, gel electrolyte, and packaging materials. These components need to have excellent flexibility and maintain stable electrochemical performance under bending and folding conditions.

Therefore, the design and development of these components are critical for the performance of flexible supercapacitors.

Flexible supercapacitors need a suitable electrolyte to achieve high energy storage performance and safe operation [15–18]. Electrolytes can be liquid, solid, or gel polymer (GPE) depending on their physical states [19]. Liquid electrolytes have high ionic conductivity, but they are flammable and need hard packaging. Solid electrolytes are safe, but they have low ionic conductivity. GPEs combine the advantages of liquid and solid electrolytes, such as high ionic conductivity, good safety, and flexibility. GPEs also have good contact and low resistance with the electrodes, as well as high stability at high temperatures [20–24]. Various types of aqueous and non-aqueous gel electrolytes have been developed for flexible supercapacitors [25–27]. Some gel electrolytes also contain redox additives that enhance the capacitance by reacting with the electrodes [28].

Polymeric hydrogel electrolytes are a type of soft electrolytes that have liquid-like ionic conductivity and solid-like elasticity [29,30]. They can replace the liquid solvents and the separator in supercapacitors, which improves the safety, corrosion resistance, and maneuverability of the devices [31,32]. However, polymeric hydrogel electrolytes still have some problems such as low ionic conductivity, weak mechanical strength, and poor electrochemical stability [33–35]. These problems limit their practical use and need to be solved by modifying the structure of the polymeric matrix [36–39]. Therefore, some recent efforts have focused on creating different functional hydrogel electrolytes with better physicochemical stabilities and mechanical strength by changing the polymeric host.

Polymeric hydrogel electrolytes need to have high ionic conductivity and mechanical strength [40,41]. Natural polysaccharides (polymeric carbohydrates) such as agar, cellulose, and carrageenan are biopolymers that can help achieve these properties. They have many hydrophilic groups that can absorb polar solvents, interact with salt ions, and regulate the viscosity of the polymer matrix. Therefore, we propose that combining physically cross-linked polysaccharides (such as agar) with a covalently cross-linked main matrix into a dual network hydrogel electrolyte can improve the performance of the polymer hydrogel electrolytes [42,43]. This is because the dual network can combine the different physicochemical properties of the two types of polymeric chains.

Chia seed (*Salvia hispanica* L.) is a crop that has many nutritional and functional benefits [44–46]. When chia seeds are soaked in water, they produce a transparent sticky gel that sticks to the seed coat [47]. This gel is called chia seed gum and it is a branched polysaccharide with a high molecular weight (between 0.8 and  $2.0 \times 10^6$  Da) [48]. The polysaccharide is made of carbohydrates with many branches that contain different types of sugar units such as L-arabinose, D-xylose, D-galactose, L-rhamnose, and galacturonic acid [49]. This complex carbohydrate is also known as mucilage.

This study aims to prepare and characterize chia mucilage gel and its electrochemical properties as a gel electrolyte. The chia mucilage gel was obtained, and its rheological and thermal properties were measured using a rheometer and TGA equipment. An EDLC with a mucilage gel electrolyte layer, flexible carbon fabric as a current collector, and two activated carbon electrodes as an active material was fabricated and tested for its electrochemical performance. The electrochemical properties were compared with the conventional salt-based electrolyte using cyclic voltammetry (CV), galvanostatic charge–discharge (GCD), and electrochemical impedance spectroscopy (EIS). The electrochemical analysis was further performed by varying the input parameters. The applicability of the supercapacitor with the mucilage gel electrolyte was evaluated via the stability test using Coulombic efficiency, CV, and EIS. The biodegradability was also verified to highlight the potential of developing biodegradable supercapacitor. The chia mucilage gel electrolyte can meet the demand for flexible electronics with the plant-driven gel material.

## 2. Materials and Methods

### 2.1. Materials

Chia seeds were purchased from the local market which produced the mucilage. Carbon-activated (AC) powder (Daejung Chemicals and Metals, Siheung, Republic of Korea) was purchased. Super P carbon and carbon foam sheet (Porous C) (MTI Corporation, Richmond, CA, USA) were purchased. Poly (vinylidene fluoride) (PVdF-(C<sub>2</sub>H<sub>2</sub>F<sub>2</sub>)<sub>n</sub>) and sodium sulfate (Na<sub>2</sub>SO<sub>4</sub>) (Sigma-Aldrich, St. Louis, MO, USA) were purchased. Whatman filter paper (Whatman plc, Kent, UK) was utilized as a separator. Deionized (DI) water was produced within the laboratory with MEGA PLUS I (Purescience, Seongnam, Republic of Korea).

### 2.2. Extraction of Mucilage and Preparation of Gel Electrolyte

Chia seeds were hydrated in water at a 1:20 ratio at 50 °C and mixed on a magnetic stirrer for 2 h. The obtained viscous solution was transferred to the conical centrifuge tubes and then the gel extraction was carried out by centrifugation at 14,000×g for 2 h with Combi R515 (Hanil Scientific Inc., Daejeon, Republic of Korea). After centrifugation, three different layers were observed in the test tubes. The top layer of seeds and excess water, including some of the soluble polysaccharide fraction, was removed. The middle layer was the mucilage gel to be extracted and was collected and prepared for the gel electrolyte. The remaining chia seeds at the bottom of the test tubes, with some remaining mucilage, were discarded. The gel electrolyte was prepared by adding 1 M of Na<sub>2</sub>SO<sub>4</sub> salt aqueous electrolyte into the extracted mucilage gel on a magnetic stirrer for 5 min. To avoid acid hydrolysis due to acid electrolytes or reduced rigidity from alkaline electrolytes in chia seed mucilage, Na<sub>2</sub>SO<sub>4</sub> was chosen as the neutral salt to provide ions in the gel electrolyte [50–52].

### 2.3. Fabrication of Activated Carbon Electrode and Coin Cell Supercapacitor

The electrodes were prepared by mixing 80% of AC, 10% of carbon black, and 10% PVDF in the mortar, and a few drops of N-Methyl-2-pyrrolidone were poured into it. The slurry was coated onto carbon fabric electrodes and dried in the convention oven at 80 °C for 24 h. The mass of the active material coated on the Ni foam (NF) is determined to be 5.25 mg. The electrode was cut into circles with a diameter of 1.5 cm to fabricate supercapacitor with coin cell. The as-fabricated carbon electrodes were immersed in 1 M Na<sub>2</sub>SO<sub>4</sub> aqueous solution for 3 h to promote the adsorption of electrolyte molecules in the electrode. The filter paper was cut into circles of 17 mm diameter. The assembly symmetric supercapacitor coin cells consist of a CR2032-positive and -negative case, wave springs, spacers, two activated carbon electrodes, mucilage gel electrolyte, and a filter paper. Each component was placed sequentially in a hydraulic crimper, MSK-110 (MTI Corporation, CA, USA), and sealed at a pressure of 50 kg cm<sup>-2</sup>.

### 2.4. Characterization

#### 2.4.1. Electrochemical Performance

An IviumStat electrochemical instrument (Ivium Technologies, North Brabant, The Netherlands) was utilized to study the electrochemical performance of supercapacitor. Cyclic voltammetry (CV) was measured within a voltage range from 0.6 to 1.8 V at a scan rate of 50 mV s<sup>-1</sup> and within a voltage range of 0–1.6 V at various scan rates from 5 mV s<sup>-1</sup> to 250 mV s<sup>-1</sup>. Galvanostatic charge–discharge (GCD) was carried out in the voltage range from 0.6 to 1.8 V at a current of 1 mA and in a voltage range of 0–1.6 V at a current density of 50, 75, 100, 150, 200, 250, and 300 mA g<sup>-1</sup>, respectively. Electrochemical impedance spectroscopy (EIS) was conducted with an AC amplitude of 10 mV and a frequency range from 40 kHz to 100 mHz.

#### 2.4.2. Optical Analysis

ALPHA II compact Fourier-transform infrared (FT-IR) Spectrometer (Bruker Corporation, Billerica, MA, USA) was used to attain the FT-IR spectrum of the mucilage film. For

measuring, the Platinum ATR (attenuated total reflection) with a single reflection diamond ATR accessory was used. The spectrum was scanned from  $4000\text{ cm}^{-1}$  to  $400\text{ cm}^{-1}$  with  $4\text{ cm}^{-1}$ -resolution.

#### 2.4.3. Rheological Gel Characterization

The behavior of chia gels under different types of stress was examined by applying shear, frequency, and amplitude sweeps with a MCR 300 Rheometer (Anton Paar GmbH, Graz, Austria). The rheometer consisted of a TEK 150-P measuring cell and a CC25 Couette geometry. The temperature was maintained at  $25\text{ }^{\circ}\text{C}$  using a Peltier element. Shear rate tests were done at shear rates ranging from 0.1 to  $100\text{ s}^{-1}$ . Frequency tests were done at frequencies from 0.1 to  $10\text{ rad s}^{-1}$  with an amplitude of 1%. Amplitude tests were done with deformations from 0.1 to 10% at a frequency of  $1\text{ rad s}^{-1}$ . The rheological properties of the newly obtained gel and mucilage electrolytes were measured.

#### 2.4.4. Thermogravimetric Analysis (TGA)

TGA was performed by TA 2950 (TA Instruments, New Castle, DE, USA). The samples were about 10 mg in a sealed aluminum pan. The scope of the testing temperature was from  $30\text{ }^{\circ}\text{C}$  to  $700\text{ }^{\circ}\text{C}$  at a heating rate of  $10\text{ }^{\circ}\text{C min}^{-1}$  under nitrogen flow of  $100\text{ mL min}^{-1}$ .

### 3. Results

Mucilage gel was extracted from chia seeds to prepare the plant-derived gel electrolyte for energy storage devices. The schematic diagram of mucilage extraction procedure is as shown in Figure 1a. The detailed process was mentioned in the experimental section. The mucilage from chia seeds is composed of Chia seed gum, which is mainly composed of xylose, glucose, and methyl glucuronic acid that form a branched polysaccharide. The branched polymer supports trapping the liquid electrolytes to improve the ionic conductivity. To extract mucilage from chia seeds, first, chia seeds were hydrated and stirred for 2 h to form the gel; after that, centrifugation was performed for 2 h to extract the gel from the solution. After centrifugation, three different layers were formed, and a gel layer was collected to utilize as gel electrolyte and the residual chia seeds at the bottom of the test tubes were discarded. The extracted gel was dried via vacuum filtration using the PTFE membrane for 24 h and the dried mucilage film was obtained. The resultant mucilage film was investigated microscopically as shown in Figure 1b. A scanning electron microscope was employed to investigate the microstructure of the mucilage surface in Figure 1c and observed the homogeneous surface. The inset shows the optical image of mucilage gel before drying.

The FT-IR spectra confirmed the chemical composition and structure of chia seed mucilage by exhibiting several characteristic peaks, shown in Figure 1d. The -OH groups of polysaccharides and water molecules, as well as the moisture content, were indicated by a broad peak at  $3288\text{ cm}^{-1}$ . The C-H stretching in methyl and methylene groups of the sugar units was evidenced by a peak at  $2921\text{ cm}^{-1}$ . The asymmetric stretching of C-O-C of 1–4 glycosidic bond ring vibrations, which suggested the presence of linear polysaccharides, was observed at  $1030\text{ cm}^{-1}$ . The carboxyl groups of uronic acid or the presence of proteins in the mucilages, which indicated its acidic and complex nature, were revealed by peaks at  $1593\text{ cm}^{-1}$  and  $1412\text{ cm}^{-1}$ . The former peak was dominated by the chia protein's secondary structures (amide I for C=O stretch) and the protein moieties present in galactomannan, while the latter peak corresponded to the symmetrical COO-link vibrations. The carboxylic acid, which could be a result of the oxidation of chia mucilage during extraction or storage, was assigned to a peak at  $1739\text{ cm}^{-1}$ . The occurrence of anomeric configurations such as CH oscillations of  $\alpha$  and  $\beta$  conformers and glycosidic linkages, attributed to  $\alpha$ -D-galactopyranose units and  $\beta$ -D-mannopyranose units, was detected between  $800$  and  $900\text{ cm}^{-1}$ . The crystallinity of chia mucilage, which reflected the intermolecular interactions and packing of the polysaccharide chains, was associated with the region between  $700$  and  $500\text{ cm}^{-1}$ .

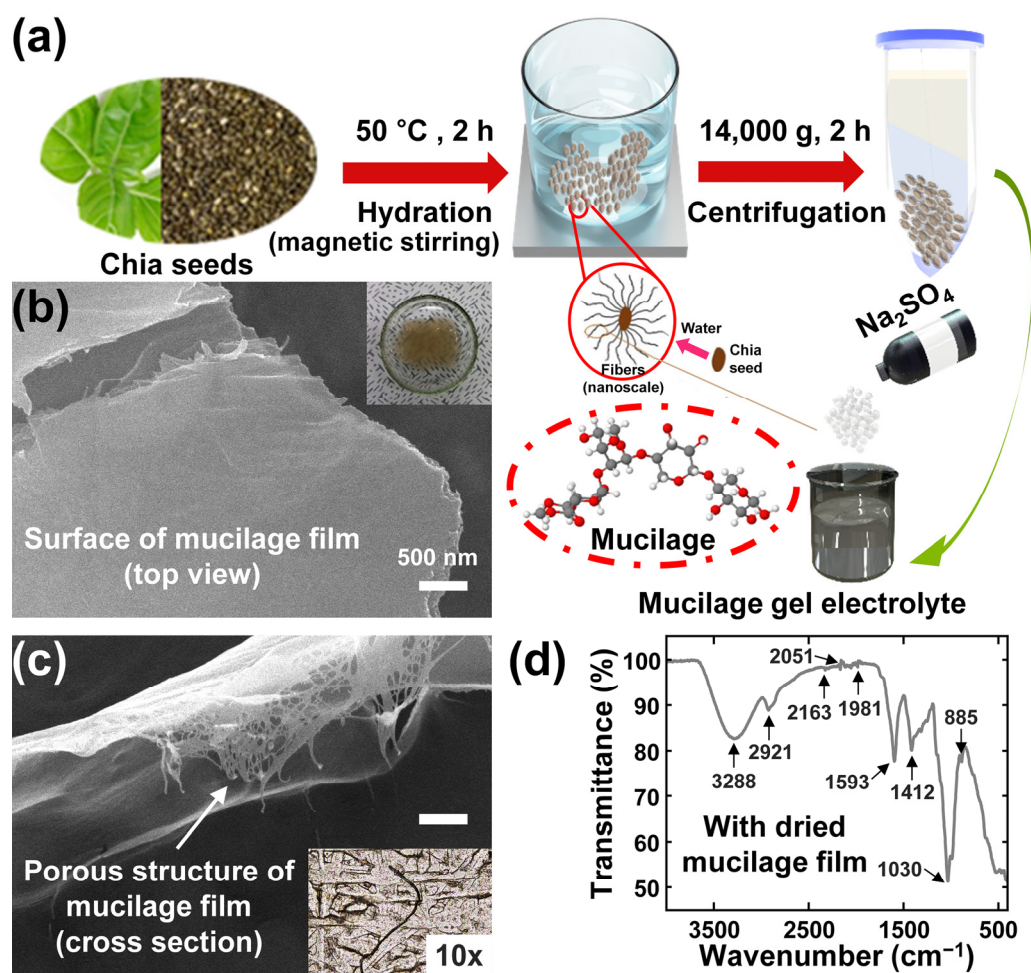


**Figure 1.** Mucilage fabrication process and material characterization: (a) Chia mucilage formation and extraction procedure; SEM images of (b) top view (inset: digital camera image of the mucilage gel) and (c) cross section view (inset: OM image of the mucilage surface) with the mucilage film; (d) FT-IR spectrum of the mucilage film.

Thermogravimetric analysis (TGA) was performed on mucilage and mucilage electrolyte, and the curves of both solutions are shown in Figure 2a. The weight loss of mucilage and mucilage electrolyte are 64.56% and 88.67%. The weight loss of mucilage gel electrolyte is enhanced after incorporation of salt  $\text{Na}_2\text{SO}_4$  compared to only mucilage gel. As a result, the thermal stability of the mucilage gel electrolyte is improved by 37%. The simple rheological property test was conducted in the upside down state of the mucilage gel container in Figure S1 and the inset of Figure 2a. After 24 h of fabrication, the mucilage was in the non-flowing state, unlike the 0 h-state. Moreover, the rheological properties of mucilage and mucilage electrolyte were characterized. In general, the mucilage solutions behave as shear thinning fluids, which means that their viscosity decreases as the rate of deformation increases in the shear direction due to the disentanglements of chain-like macro-molecules. Figure 2b depicts the graph showing the steady shear viscosity change as a function of the shear rate, which ranges from 0.1 to  $100 \text{ s}^{-1}$ . As a result, the graph for both solutions indicates that the viscosity is decreasing with the increase in shear rate, resulting in shear thinning behavior. Moreover, the dynamic frequency sweep of mucilage and mucilage electrolyte are also shown in Figure 2c, and the storage modulus  $G'$  and loss modulus  $G''$  were determined through shear flows at frequencies ranging from 0.1 to  $10 \text{ rad s}^{-1}$ . Furthermore, dynamic strain sweeps were performed, and the storage modulus  $G'$  and loss modulus  $G''$  were determined for the mucilage and mucilage electrolyte at a constant frequency of  $10 \text{ rad s}^{-1}$ . For all rheological measurements, the viscoelastic properties of mucilage and

the mucilage electrolyte are reported as similar to the previous research. Therefore, the extracted mucilage gel is utilized to fabricate gel electrolyte for supercapacitor application.

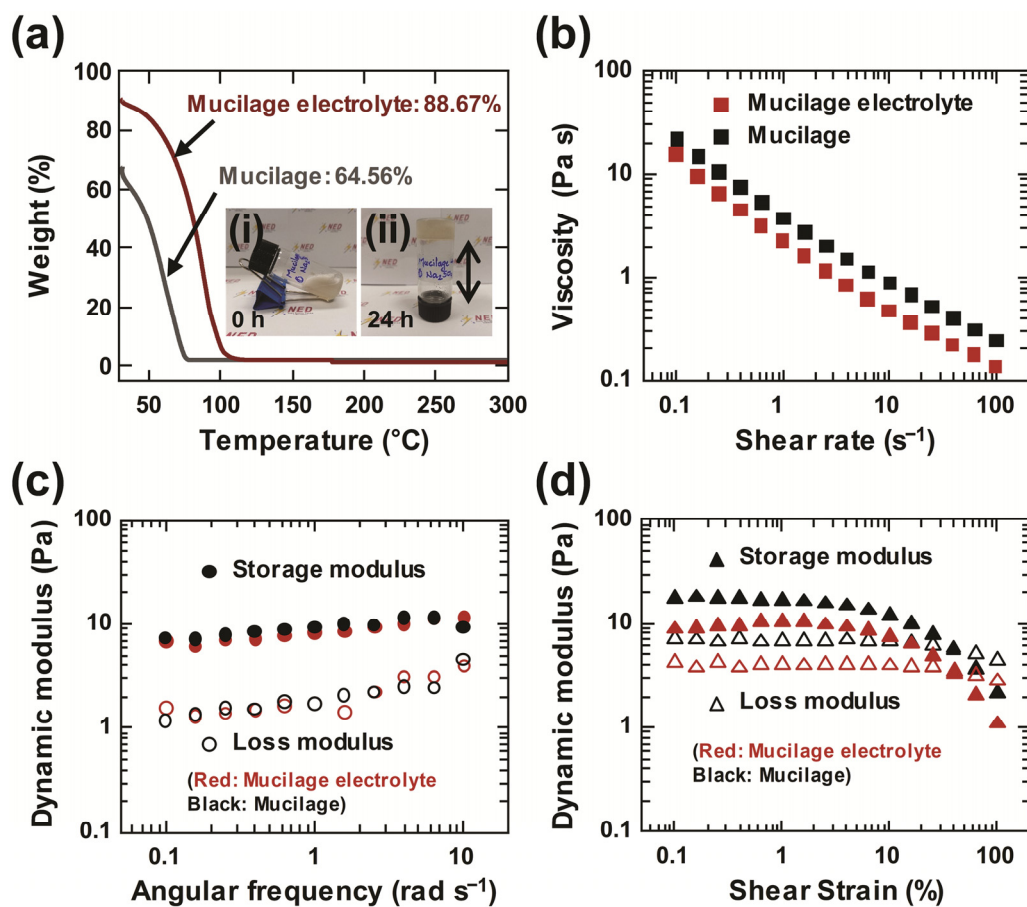


**Figure 2.** Thermal and rheological analysis of the mucilage gel: (a) thermogravimetric analysis of mucilage and mucilage electrolyte (inset (i): initial stage of the mucilage gel; inset (ii): upside down state of the mucilage after 24 h); (b) change of steady shear viscosity as a function of shear rate; (c) dynamic frequency sweeps; and (d) dynamic strain sweeps for mucilage and mucilage electrolyte.

The symmetric supercapacitor was assembled using two activated carbon electrodes, mucilage gel electrolyte, and a filter paper as a separator, as shown Figure 3a. The electrodes were prepared by mixing activated carbon, carbon black, PVDF, and a few drops of N-Methyl-2-pyrrolidone. Then, the slurry was coated and dried onto carbon fabric electrodes. The SEM image of the fabricated electrode layer can be seen in Figure S2a. The electrode was cut into a 1.5 cm circular shape and displayed in Figure S2b. Chia seeds were hydrated in water, and the gel extraction was carried out by centrifugation at  $14,000 \times g$  for 2 h. After centrifugation, three different layers were observed in the test tubes and the middle layer (mucilage gel) was extracted. The mucilage gel electrolyte was prepared by adding 1 M of Na<sub>2</sub>SO<sub>4</sub> aqueous electrolyte into the extracted mucilage gel. The control sample (salt electrolyte supercapacitor) was assembled as similarly to the mucilage gel electrolyte supercapacitor, with two activated carbon electrodes, a filter paper, and 1 M of Na<sub>2</sub>SO<sub>4</sub> aqueous electrolyte. To evaluate the enhancement of the mucilage gel electrolyte on the supercapacitor performance, CV, GCD, and EIS were conducted. In Figure 3b, the CV curves of the supercapacitors were recorded in the voltage range from 0 V to +1.0 V at a scan rate of 50 mV s<sup>-1</sup>. The mucilage gel electrolyte supercapacitor had a more stable potential window than the salt electrolyte supercapacitor. The CV curve of the salt electrolyte supercapacitor showed oxidation, while the CV curve of the mucilage gel electrolyte supercapacitor

remained rectangular, indicating an ideal carbon-based symmetric supercapacitor. The specific capacitance of both supercapacitors was calculated using Equations (1) and (2):

$$C_p = (\int I \times \Delta V) / (m \times v \times \Delta V), \quad (1)$$

$$C_p = (I \times \Delta t) / (m \times \Delta V), \quad (2)$$

where  $C_p$ ,  $I$ ,  $\Delta t$ ,  $m$ ,  $v$ , and  $\Delta V$  are specific capacitance, output current, time for measuring one cycle, mass of electrode material, scan rate, and potential window, respectively [53]. The mucilage gel-case had a longer discharge time (22.4 s) than the salt-case (20.5 s), which was 9.27% higher. The Nyquist plot in Figure 3d shows that the charge transfer process was faster in the mucilage gel-case than in the salt-case, based on the slope of the plot. Due to the presence of polysaccharides in the chia seed mucilage gel, the electrochemical performance is enhanced, exhibiting greater ionic conductivity compared to the standalone  $\text{Na}_2\text{SO}_4$  electrolyte [54].

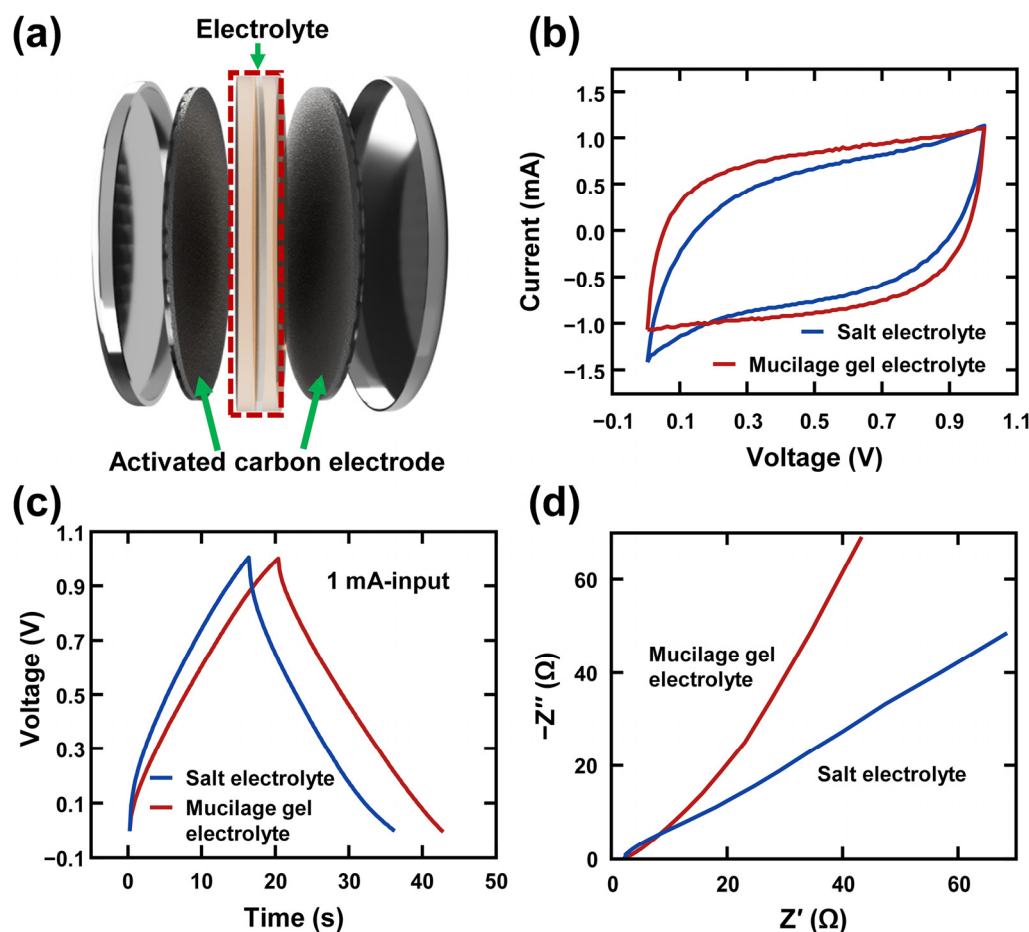


**Figure 3.** Basic electrochemical performance of mucilage gel supercapacitor: (a) schematic diagram of symmetric supercapacitor using mucilage gel electrolyte; comparison of activated carbon-based symmetric supercapacitor between salt electrolyte and mucilage gel electrolyte with (b) cyclic voltammetry (CV) curves, (c) galvanostatic charge–discharge (GCD) curves, and (d) Nyquist plot.

Figures 4 and 5 show the electrochemical performance results in detail. The optimal potential window of the supercapacitor was determined by examining the CV curves at various potential windows from 0–0.6 V to 0–1.8 V in Figure 4a. The figure shows that all the CV curves maintained their original shape without any distortion up to 0–1.8 V and did not exhibit a sharp peak for the potential window (due to the oxygen/hydrogen evolution). To achieve a stable output curve, the 0–1.6 V range was chosen as the appropriate potential

window for further analysis. Figure 4b displays the CV curves of the HSC device at different scan rates from 50 to 250 mV s<sup>-1</sup>. The CV curves have rectangular shapes because of the electric double layer type materials in the device. The specific capacitance values were computed for each scan rate from CV curves and plotted in Figure 4c. The specific capacitances of the device are 10.76, 10.04, 9.57, 9.11, and 8.69 F g<sup>-1</sup> for scan rates of 50, 100, 150, 200, and 250 mV s<sup>-1</sup>, respectively.

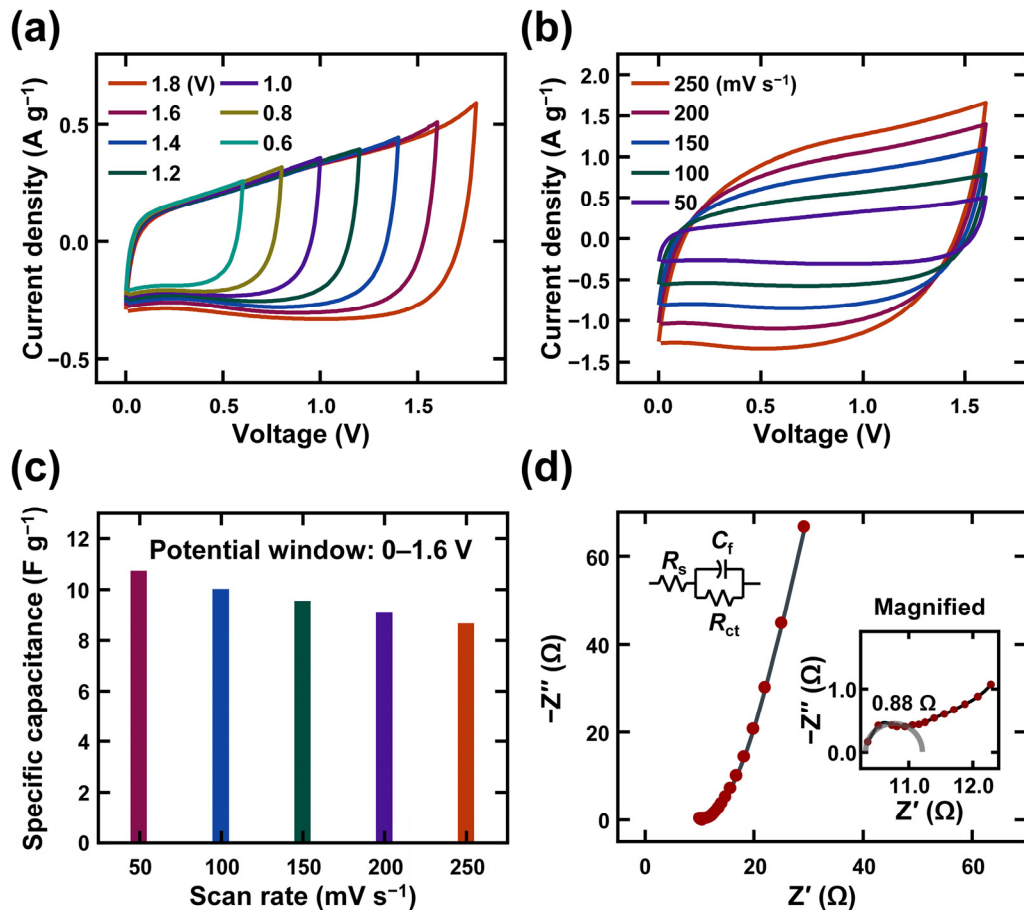


**Figure 4.** Electrochemical performance of mucilage gel supercapacitor based on CV and EIS: (a) CV curves according to different potential window; (b) CV curves according to different scan rates from 50 mV s<sup>-1</sup> to 250 mV s<sup>-1</sup>; (c) specific capacitance of the mucilage gel supercapacitor; (d) Nyquist plot of mucilage gel supercapacitor with EIS from 40 kHz to 100 mHz (insets: magnified graph of EIS result and equivalent circuit).

Figure 4d shows the electrochemical impedance spectroscopy results to evaluate the equivalent series resistance of the hybrid nanocomposite electrodes before and after the cycling stability test. The internal resistance of the device ( $R_s$ ) is obtained from the X-axis-intercepting point of the Nyquist plot with 10.33 Ω [55]. This value includes the internal resistance of the active material, the electrolyte resistance, and the contact resistance between the current collector and the active electrode material. The charge transfer resistance ( $R_{ct}$ ) stands at 0.76 Ω, ascertained from the diameter of the semicircle in the high-middle frequency region. The low value of R1 is attributed to the conductive gel electrolyte with chia seed mucilage.

The device was also tested by changing the voltage range from 0.6 to 1.8 V at a constant current density of 180 mA g<sup>-1</sup> and recording the GCD curves in Figure 5a. The figure shows that clear triangular shapes were obtained at lower potentials, where the capacitive mechanism is dominant and the shape slightly changed with increasing the potential range, indicating the coexistence of capacitive and EDLC-type mechanisms. Based

on the CV and GCD curves at different potentials, 1.6 V was selected as stable potential, and detailed electrochemical analysis of the device was performed at this potential. The GCD measurements were conducted at a fixed potential range of 0–1.6 V by changing the current densities from 60 to 350 mA g<sup>-1</sup> (Figure 5b). The specific capacitance values were computed using Equation (2) for each current density from the GCD curves and plotted in Figure 5c. The specific capacitances of the device are 7.77, 7.44, 7.13, 6.77, 6.5, 6.26, and 6.07 F g<sup>-1</sup> for the current densities of 60, 90, 120, 180, 240, 300, and 360 mA g<sup>-1</sup>, respectively. Moreover, the areal energy density and power density of the device were calculated using Equations (3) and (4) and presented in Figure 5d.

$$E_d = 0.5 \times (C_p \times \Delta V^2 \times 1000)/3600, \quad (3)$$

$$P_d = E_d \times 3600/\Delta t, \quad (4)$$

where  $E_d$  and  $P_d$  stand for energy density and power density, respectively [53]. The device showed a high energy density of 2.763 Wh kg<sup>-1</sup> at a power density of 48 W kg<sup>-1</sup>. Moreover, the device performed well under high current density of 360 mA g<sup>-1</sup>, with a specific energy density of 2.158 Wh kg<sup>-1</sup> at a high power density of 287.7 W kg<sup>-1</sup>. The energy density and power density values of the current supercapacitor are within the range of symmetric supercapacitors.

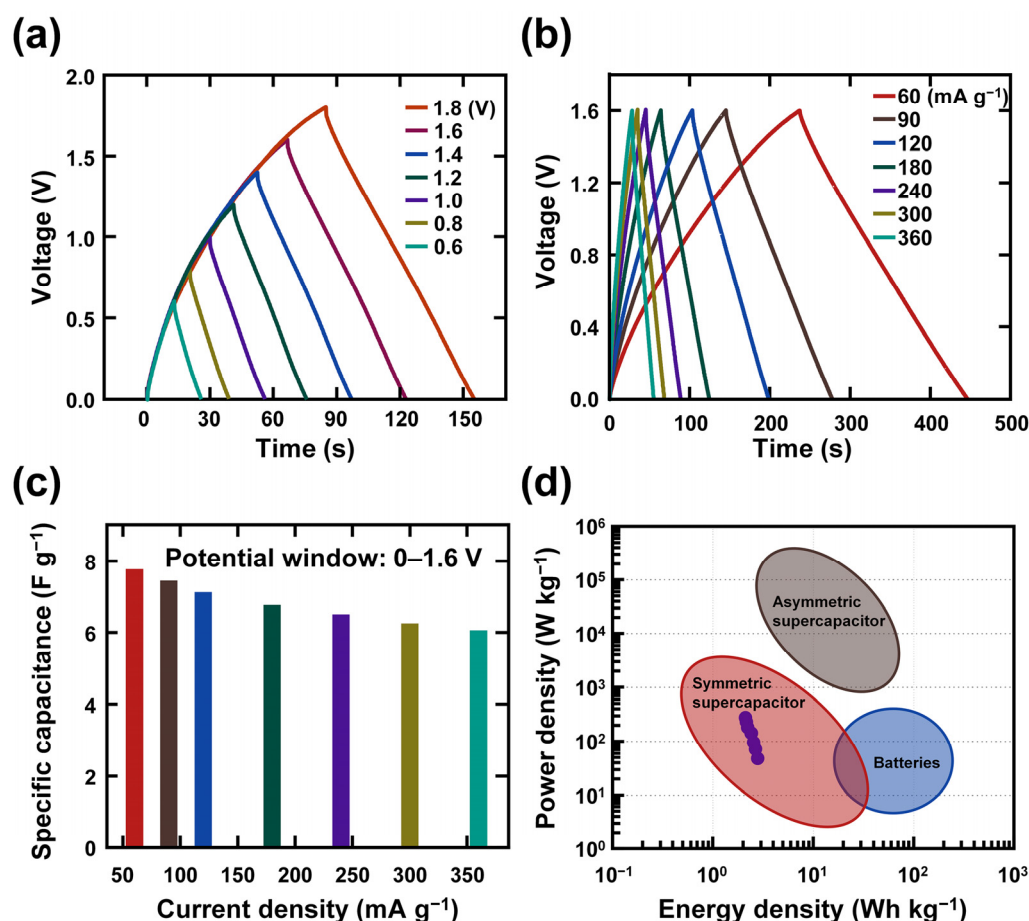


**Figure 5.** Electrochemical performance of mucilage gel supercapacitor based on GCD: (a) GCD curves according to different potential window; (b) GCD analysis according to different current densities from 60 mA g<sup>-1</sup> to 360 mA g<sup>-1</sup>; (c) specific capacitance of the mucilage gel supercapacitor; (d) Ragone plot of the mucilage gel supercapacitor.

Figure 6 shows the applicability of the mucilage gel electrolyte. The electrode exhibited good stability during the test, with a remarkable capacity retention of 94% at the end of

10,000th cycle with the current density of  $750 \text{ mA g}^{-1}$ , as shown in Figure 6a. The capacity retention result implies that the supercapacitor with the mucilage gel electrolyte can preserve the discharge time even after 10,000 cycles. The detailed five peaks are displayed in the inset of Figure 6a. To demonstrate the high energy density and power density of the device, it was tested for its feasibility by lighting up a commercial orange LED. Figure 6b shows that the device successfully lit up the LED for 40 s after charging for a while. The comparison before and after the stability test was performed with EIS and CV curve measurements in Figure 6c,d, respectively. The charge transfer resistance value of  $0.96 \Omega$  after cycling in Figures 6c and S3 showed a slight increase in the values after long-term operations compared to that of  $0.88 \Omega$  before long-term operations in the inset of Figure 4d. The current density of the CV curve in Figure 6d also showed a slight decrease after long-term operations. Both results indicated that the fabricated mucilage-based electrolyte is stable even in a gel state.

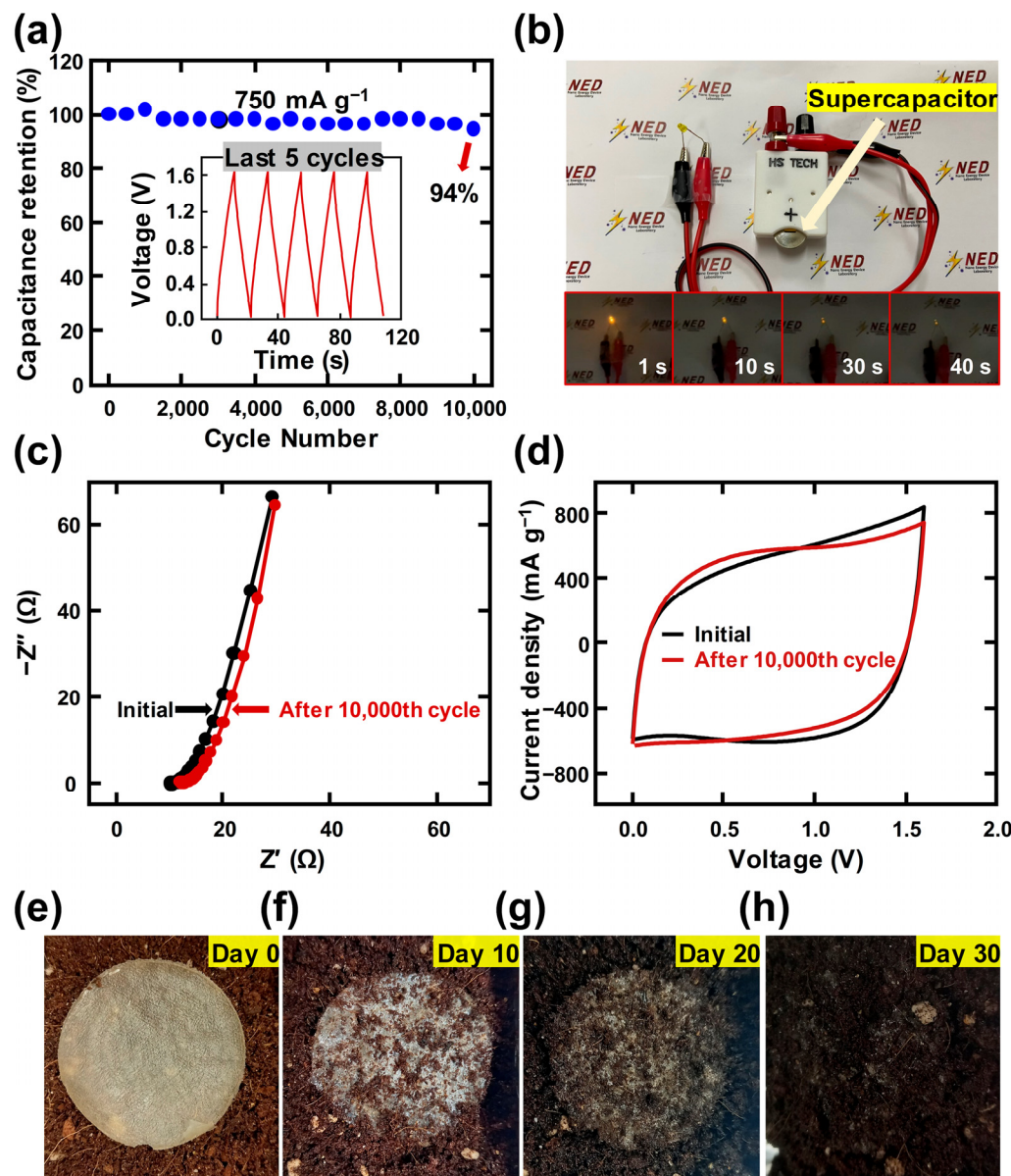


**Figure 6.** Output stability of mucilage gel supercapacitor and biodegradability assessment of the fabricated film: (a) cycling stability of the mucilage gel supercapacitors (inset: outputs from the last

five cycles of the stability test); (b) lighting up LED with the as-fabricated mucilage gel supercapacitor with the lighting time from 1 to 40 s; (c) electrochemical impedance spectroscopy (EIS) curves and (d) CV curves at 100 mV s<sup>-1</sup> of mucilage gel supercapacitor (the initial and after 10,000th cycle of the charging/discharging time); (e–h) biodegradability test of the mucilage film from 0 to 30 days.

The mucilage gel electrolyte can exhibit biodegradability because it is derived from a natural polymer. The electrolyte layer was put on the soil in a 3D printed container at room temperature. The layer began to decompose after 10 days and completely degraded after 30 days without applying mechanical input, as shown in Figure 6e–h. Table 1 displays the summarized electrochemical performance of the proposed device. The mucilage gel electrolyte can be used to fabricate a sustainable supercapacitor with an environmentally friendly approach.

**Table 1.** The summary of output results with the proposed device.

Potential Window (V)	Highest Output Current (mA)	Input Current Density (A g <sup>-1</sup> )	Energy Density (Wh kg <sup>-1</sup> )	Power Density (W kg <sup>-1</sup> )	Output Stability (10,000 Cycles) (%)
1.6	8.898	0.06–0.36	2.158–2.763	48–287.7	94

#### 4. Conclusions

In summary, the chia mucilage gel was prepared and characterized for its rheological, thermal, and electrochemical properties. The chia mucilage gel was obtained via hydration and centrifugation. The chemical structure of the dried chia mucilage gel was verified via the FT-IR spectrum. The mucilage gel electrolyte exhibited high thermal stability and shear thinning behavior, as shown by TGA and the rheological study. An EDLC with symmetric AC electrodes was fabricated and tested for its electrochemical performance. The mucilage gel electrolyte had a more rectangular shape in the CV curve, longer discharging time, and lower charge transfer resistance than the salt-based electrolyte. The electrochemical properties were further investigated by varying the potential window, scan rate, and input current. A maximum specific capacitance of 7.77 F g<sup>-1</sup> and an energy density of 2.76 Wh kg<sup>-1</sup> were achieved with a potential window of 1.6 V and an input current density of 60 mA g<sup>-1</sup>. The highest power density of 287.7 W kg<sup>-1</sup> was obtained with input current density of 360 mA g<sup>-1</sup>, and the results with the two density values were within the range of symmetric supercapacitor in the Ragone plot. To demonstrate the applicability of the chia mucilage gel electrolyte, stable capacitance retention of 94% after 10,000 cycles of high-input-current condition and similar CV/EIS results before and after the stability test were observed. In addition, an orange-colored LED was powered by the EDLC for 40 s after charging. The biodegradability of the mucilage film was also confirmed by the degraded image after 30 days in a soil environment. This study suggests that plant-driven gel materials can be used to enhance the applicability of the flexible gel electrolyte-based supercapacitor.

**Supplementary Materials:** The following supporting information can be downloaded at <https://www.mdpi.com/article/10.3390/batteries9100512/s1>: Figure S1: Digital camera images of chia mucilage gel after 2 and 3 days; Figure S2: Images for activated carbon electrode; Figure S3: Magnified Nyquist plot for the fabricated supercapacitor after stability test.

**Author Contributions:** Conceptualization, I.K.; Methodology, I.K., S.T.S., A.C.M. and S.D.D.; Software, I.K.; Validation, I.K., A.C.M. and S.D.D.; Formal analysis, I.K., A.C.M. and S.D.D.; Investigation, I.K. and S.T.S.; Resources, D.K.; Data curation, I.K. and S.T.S.; Writing—original draft, I.K.; Writing—review and editing, I.K., A.C.M., S.D.D., S.-B.J. and D.K.; Visualization, I.K. and S.T.S.; Supervision, S.-B.J. and D.K.; Project administration, D.K.; Funding acquisition, D.K. All authors have read and agreed to the published version of the manuscript.

**Funding:** This results was supported by “Regional Innovation Strategy (RIS)” through the National Research Foundation of Korea (NRF) funded by the Ministry of Education (MOE) (2021RIS-004). This work was supported by a grant from Kyung Hee University in 2020 (KHU-20201109).

**Data Availability Statement:** Not applicable.

**Conflicts of Interest:** The authors declare no conflict of interest.

## References

- Huang, Q.; Wang, D.; Zheng, Z. Textile-Based Electrochemical Energy Storage Devices. *Adv. Energy Mater.* **2016**, *6*, 1600783. [[CrossRef](#)]
- Liu, Y.; He, K.; Chen, G.; Leow, W.R.; Chen, X. Nature-Inspired Structural Materials for Flexible Electronic Devices. *Chem. Rev.* **2017**, *117*, 12893–12941. [[CrossRef](#)] [[PubMed](#)]
- Yang, Y.; Gao, W. Wearable and Flexible Electronics for Continuous Molecular Monitoring. *Chem. Soc. Rev.* **2019**, *48*, 1465–1491. [[CrossRef](#)]
- Low, Z.W.K.; Li, Z.; Owh, C.; Chee, P.L.; Ye, E.; Kai, D.; Yang, D.-P.; Loh, X.J. Using Artificial Skin Devices as Skin Replacements: Insights into Superficial Treatment. *Small* **2019**, *15*, 1805453. [[CrossRef](#)]
- Ma, Z. An Electronic Second Skin. *Science* **2011**, *333*, 830–831. [[CrossRef](#)]
- Shi, J.; Liu, S.; Zhang, L.; Yang, B.; Shu, L.; Yang, Y.; Ren, M.; Wang, Y.; Chen, J.; Chen, W.; et al. Smart Textile-Integrated Microelectronic Systems for Wearable Applications. *Adv. Mater.* **2020**, *32*, 1901958. [[CrossRef](#)] [[PubMed](#)]
- Chen, D.; Pei, Q. Electronic Muscles and Skins: A Review of Soft Sensors and Actuators. *Chem. Rev.* **2017**, *117*, 11239–11268. [[CrossRef](#)]
- Xu, W.; Liu, C.; Wu, Q.; Xie, W.; Kim, W.-Y.; Lee, S.-Y.; Gwon, J. A Stretchable Solid-State Zinc Ion Battery Based on a Cellulose Nanofiber-Polyacrylamide Hydrogel Electrolyte and a Mg<sub>0.23</sub>V<sub>2</sub>O<sub>5</sub>·1.0H<sub>2</sub>O Cathode. *J. Mater. Chem. A* **2020**, *8*, 18327–18337. [[CrossRef](#)]
- Huang, J.; Zhao, B.; Liu, T.; Mou, J.; Jiang, Z.; Liu, J.; Li, H.; Liu, M. Wood-Derived Materials for Advanced Electrochemical Energy Storage Devices. *Adv. Funct. Mater.* **2019**, *29*, 1902255. [[CrossRef](#)]
- Li, X.; Yuan, L.; Liu, R.; He, H.; Hao, J.; Lu, Y.; Wang, Y.; Liang, G.; Yuan, G.; Guo, Z. Engineering Textile Electrode and Bacterial Cellulose Nanofiber Reinforced Hydrogel Electrolyte to Enable High-Performance Flexible All-Solid-State Supercapacitors. *Adv. Energy Mater.* **2021**, *11*, 2003010. [[CrossRef](#)]
- Xu, T.; Du, H.; Liu, H.; Liu, W.; Zhang, X.; Si, C.; Liu, P.; Gaynor, K.M. Advanced Nanocellulose-Based Composites for Flexible Functional Energy Storage Devices. *Adv. Mater.* **2021**, *33*, 2101368. [[CrossRef](#)]
- Zhang, L.L.; Zhao, X.S. Carbon-Based Materials as Supercapacitor Electrodes. *Chem. Soc. Rev.* **2009**, *38*, 2520. [[CrossRef](#)] [[PubMed](#)]
- Wang, G.; Zhang, L.; Zhang, J. A Review of Electrode Materials for Electrochemical Supercapacitors. *Chem. Soc. Rev.* **2012**, *41*, 797–828. [[CrossRef](#)]
- Zhong, C.; Deng, Y.; Hu, W.; Qiao, J.; Zhang, L.; Zhang, J. A Review of Electrolyte Materials and Compositions for Electrochemical Supercapacitors. *Chem. Soc. Rev.* **2015**, *44*, 7484–7539. [[CrossRef](#)]
- Zang, L.; Liu, Q.; Qiu, J.; Yang, C.; Wei, C.; Liu, C.; Lao, L. Design and Fabrication of an All-Solid-State Polymer Supercapacitor with Highly Mechanical Flexibility Based on Polypyrrole Hydrogel. *ACS Appl. Mater. Interfaces* **2017**, *9*, 33941–33947. [[CrossRef](#)]
- Wen, L.; Li, F.; Cheng, H.-M. Carbon Nanotubes and Graphene for Flexible Electrochemical Energy Storage: From Materials to Devices. *Adv. Mater.* **2016**, *28*, 4306–4337. [[CrossRef](#)] [[PubMed](#)]
- Karaman, B.; Çevik, E.; Bozkurt, A. Novel Flexible Li-Doped PEO/Copolymer Electrolytes for Supercapacitor Application. *Ionics* **2019**, *25*, 1773–1781. [[CrossRef](#)]
- Cevik, E.; Bozkurt, A.; Dirican, M.; Zhang, X. High Performance Flexible Supercapacitors Including Redox Active Molybdate Incorporated Poly(Vinylphosphonic Acid) Hydrogels. *Int. J. Hydrol. Energy* **2020**, *45*, 2186–2194. [[CrossRef](#)]
- Ngai, K.S.; Ramesh, S.; Ramesh, K.; Juan, J.C. A Review of Polymer Electrolytes: Fundamental, Approaches and Applications. *Ionics* **2016**, *22*, 1259–1279. [[CrossRef](#)]
- Hou, J.; Liu, M.; Zhang, H.; Song, Y.; Jiang, X.; Yu, A.; Jiang, L.; Su, B. Healable Green Hydrogen Bonded Networks for Circuit Repair, Wearable Sensor and Flexible Electronic Devices. *J. Mater. Chem. A* **2017**, *5*, 13138–13144. [[CrossRef](#)]
- Qin, K.; Liu, E.; Li, J.; Kang, J.; Shi, C.; He, C.; He, F.; Zhao, N. Free-Standing 3D Nanoporous Duct-Like and Hierarchical Nanoporous Graphene Films for Micron-Level Flexible Solid-State Asymmetric Supercapacitors. *Adv. Energy Mater.* **2016**, *6*, 1600755. [[CrossRef](#)]
- Wang, J.; Chen, G.; Song, S. Na-Ion Conducting Gel Polymer Membrane for Flexible Supercapacitor Application. *Electrochim. Acta* **2020**, *330*, 135322. [[CrossRef](#)]
- Mantravadi, R.; Chinnam, P.R.; Dikin, D.A.; Wunder, S.L. High Conductivity, High Strength Solid Electrolytes Formed by in Situ Encapsulation of Ionic Liquids in Nanofibrillar Methyl Cellulose Networks. *ACS Appl. Mater. Interfaces* **2016**, *8*, 13426–13436. [[CrossRef](#)] [[PubMed](#)]
- Rana, H.H.; Park, J.H.; Ducrot, E.; Park, H.; Kota, M.; Han, T.H.; Lee, J.Y.; Kim, J.; Kim, J.-H.; Howlett, P.; et al. Extreme Properties of Double Networked Ionogel Electrolytes for Flexible and Durable Energy Storage Devices. *Energy Storage Mater.* **2019**, *19*, 197–205. [[CrossRef](#)]

25. Cevik, E.; Gunday, S.T.; Bozkurt, A.; Amine, R.; Amine, K. Bio-Inspired Redox Mediated Electrolyte for High Performance Flexible Supercapacitor Applications over Broad Temperature Domain. *J. Power Sources* **2020**, *474*, 228544. [[CrossRef](#)]
26. Aziz, S.B.; Hamsan, M.H.; Brza, M.A.; Kadir, M.F.Z.; Muzakir, S.K.; Abdulwahid, R.T. Effect of Glycerol on EDLC Characteristics of Chitosan:Methylcellulose Polymer Blend Electrolytes. *J. Mater. Res. Technol.* **2020**, *9*, 8355–8366. [[CrossRef](#)]
27. Railanmaa, A.; Lehtimäki, S.; Keskinen, J.; Lupo, D. Non-Toxic Printed Supercapacitors Operating in Sub-Zero Conditions. *Sci. Rep.* **2019**, *9*, 14059. [[CrossRef](#)]
28. Cevik, E.; Bozkurt, A. Redox Active Polymer Metal Chelates for Use in Flexible Symmetrical Supercapacitors: Cobalt-Containing Poly(Acrylic Acid) Polymer Electrolytes. *J. Energy Chem.* **2021**, *55*, 145–153. [[CrossRef](#)]
29. Li, X.; Lou, D.; Wang, H.; Sun, X.; Li, J.; Liu, Y.-N. Flexible Supercapacitor Based on Organohydrogel Electrolyte with Long-Term Anti-Freezing and Anti-Drying Property. *Adv. Funct. Mater.* **2020**, *30*, 2007291. [[CrossRef](#)]
30. Zhou, Y.; Wan, C.; Yang, Y.; Yang, H.; Wang, S.; Dai, Z.; Ji, K.; Jiang, H.; Chen, X.; Long, Y. Highly Stretchable, Elastic, and Ionic Conductive Hydrogel for Artificial Soft Electronics. *Adv. Funct. Mater.* **2019**, *29*, 1806220. [[CrossRef](#)]
31. Xu, Z.; Chu, X.; Wang, Y.; Zhang, H.; Yang, W. Three-Dimensional Polymer Networks for Solid-State Electrochemical Energy Storage. *Chem. Eng. J.* **2020**, *391*, 123548. [[CrossRef](#)]
32. Dong, H.; Li, J.; Guo, J.; Lai, F.; Zhao, F.; Jiao, Y.; Brett, D.J.L.; Liu, T.; He, G.; Parkin, I.P. Insights on Flexible Zinc-Ion Batteries from Lab Research to Commercialization. *Adv. Mater.* **2021**, *33*, 2007548. [[CrossRef](#)] [[PubMed](#)]
33. Liu, Z.; Liang, G.; Zhan, Y.; Li, H.; Wang, Z.; Ma, L.; Wang, Y.; Niu, X.; Zhi, C. A Soft yet Device-Level Dynamically Super-Tough Supercapacitor Enabled by an Energy-Dissipative Dual-Crosslinked Hydrogel Electrolyte. *Nano Energy* **2019**, *58*, 732–742. [[CrossRef](#)]
34. Gong, X.; Yang, Q.; Zhi, C.; Lee, P.S. Stretchable Energy Storage Devices: From Materials and Structural Design to Device Assembly. *Adv. Energy Mater.* **2021**, *11*, 2003308. [[CrossRef](#)]
35. Wang, Z.; Li, H.; Tang, Z.; Liu, Z.; Ruan, Z.; Ma, L.; Yang, Q.; Wang, D.; Zhi, C. Hydrogel Electrolytes for Flexible Aqueous Energy Storage Devices. *Adv. Funct. Mater.* **2018**, *28*, 1804560. [[CrossRef](#)]
36. Fu, Q.; Hao, S.; Meng, L.; Xu, F.; Yang, J. Engineering Self-Adhesive Polyzwitterionic Hydrogel Electrolytes for Flexible Zinc-Ion Hybrid Capacitors with Superior Low-Temperature Adaptability. *ACS Nano* **2021**, *15*, 18469–18482. [[CrossRef](#)]
37. Chen, M.; Chen, J.; Zhou, W.; Xu, J.; Wong, C.-P. High-Performance Flexible and Self-Healable Quasi-Solid-State Zinc-Ion Hybrid Supercapacitor Based on Borax-Crosslinked Polyvinyl Alcohol/Nanocellulose Hydrogel Electrolyte. *J. Mater. Chem. A* **2019**, *7*, 26524–26532. [[CrossRef](#)]
38. Yang, G.; Huang, J.; Wan, X.; Zhu, Y.; Liu, B.; Wang, J.; Hiralal, P.; Fontaine, O.; Guo, Y.; Zhou, H. A Low Cost, Wide Temperature Range, and High Energy Density Flexible Quasi-Solid-State Zinc-Ion Hybrid Supercapacitors Enabled by Sustainable Cathode and Electrolyte Design. *Nano Energy* **2021**, *90*, 106500. [[CrossRef](#)]
39. Han, L.; Huang, H.; Fu, X.; Li, J.; Yang, Z.; Liu, X.; Pan, L.; Xu, M. A Flexible, High-Voltage and Safe Zwitterionic Natural Polymer Hydrogel Electrolyte for High-Energy-Density Zinc-Ion Hybrid Supercapacitor. *Chem. Eng. J.* **2020**, *392*, 123733. [[CrossRef](#)]
40. Lizundia, E.; Kundu, D. Advances in Natural Biopolymer-Based Electrolytes and Separators for Battery Applications. *Adv. Funct. Mater.* **2021**, *31*, 2005646. [[CrossRef](#)]
41. Zhao, S.; Zuo, Y.; Liu, T.; Zhai, S.; Dai, Y.; Guo, Z.; Wang, Y.; He, Q.; Xia, L.; Zhi, C.; et al. Multi-Functional Hydrogels for Flexible Zinc-Based Batteries Working under Extreme Conditions. *Adv. Energy Mater.* **2021**, *11*, 2101749. [[CrossRef](#)]
42. Chen, Q.; Zhu, L.; Zhao, C.; Wang, Q.; Zheng, J. A Robust, One-Pot Synthesis of Highly Mechanical and Recoverable Double Network Hydrogels Using Thermoreversible Sol-Gel Polysaccharide. *Adv. Mater.* **2013**, *25*, 4171–4176. [[CrossRef](#)]
43. Sun, J.-Y.; Zhao, X.; Illeperuma, W.R.K.; Chaudhuri, O.; Oh, K.H.; Mooney, D.J.; Vlassak, J.J.; Suo, Z. Highly Stretchable and Tough Hydrogels. *Nature* **2012**, *489*, 133–136. [[CrossRef](#)] [[PubMed](#)]
44. Punia, S.; Dhull, S.B. Chia Seed (*Salvia hispanica* L.) Mucilage (a Heteropolysaccharide): Functional, Thermal, Rheological Behaviour and Its Utilization. *Int. J. Biol. Macromol.* **2019**, *140*, 1084–1090. [[CrossRef](#)]
45. Silva, L.A.; Sinnecker, P.; Cavalari, A.A.; Sato, A.C.K.; Perrechil, F.A. Extraction of Chia Seed Mucilage: Effect of Ultrasound Application. *Food Chem.* **2022**, *1*, 100024. [[CrossRef](#)]
46. Mutlu, S.; Kopuk, B.; Palabiyik, I. Effect of Cold Atmospheric Pressure Argon Plasma Jet Treatment on the Freeze-Dried Mucilage of Chia Seeds (*Salvia hispanica* L.). *Foods* **2023**, *12*, 1563. [[CrossRef](#)]
47. Brütsch, L.; Stringer, F.J.; Kuster, S.; Windhab, E.J.; Fischer, P. Chia Seed Mucilage—A Vegan Thickener: Isolation, Tailoring Viscoelasticity and Rehydration. *Food Funct.* **2019**, *10*, 4854–4860. [[CrossRef](#)] [[PubMed](#)]
48. Tavares, L.S.; Junqueira, L.A.; de Oliveira Guimarães, Í.C.; de Resende, J.V. Cold Extraction Method of Chia Seed Mucilage (*Salvia hispanica* L.): Effect on Yield and Rheological Behavior. *J. Food Sci. Technol.* **2018**, *55*, 457–466. [[CrossRef](#)]
49. Tosif, M.M.; Najda, A.; Bains, A.; Kaushik, R.; Dhull, S.B.; Chawla, P.; Walasek-Janusz, M. A Comprehensive Review on Plant-Derived Mucilage: Characterization, Functional Properties, Applications, and Its Utilization for Nanocarrier Fabrication. *Polymers* **2021**, *13*, 1066. [[CrossRef](#)]
50. Cumpstey, I. Chemical Modification of Polysaccharides. *ISRN Org. Chem.* **2013**, *2013*, 1–27. [[CrossRef](#)]
51. Mohammed, A.S.A.; Naveed, M.; Jost, N. Polysaccharides; Classification, Chemical Properties, and Future Perspective Applications in Fields of Pharmacology and Biological Medicine (A Review of Current Applications and Upcoming Potentialities). *J. Polym. Environ.* **2021**, *29*, 2359–2371. [[CrossRef](#)] [[PubMed](#)]

52. Sun, S.; Chen, W.; Tang, J.; Wang, B.; Cao, X.; Sun, S.; Sun, R.-C. Synergetic Effect of Dilute Acid and Alkali Treatments on Fractional Application of Rice Straw. *Biotechnol. Biofuels* **2016**, *9*, 217. [[CrossRef](#)] [[PubMed](#)]
53. Shah, S.S.; Aziz, M.A.; Cevik, E.; Ali, M.; Gunday, S.T.; Bozkurt, A.; Yamani, Z.H. Sulfur Nano-Confinement in Hierarchically Porous Jute Derived Activated Carbon towards High-Performance Supercapacitor: Experimental and Theoretical Insights. *J. Energy Storage* **2022**, *56*, 105944. [[CrossRef](#)]
54. Gough, C.R.; Rivera-Galletti, A.; Cowan, D.A.; Salas-de La Cruz, D.; Hu, X. Protein and Polysaccharide-Based Fiber Materials Generated from Ionic Liquids: A Review. *Molecules* **2020**, *25*, 3362. [[CrossRef](#)] [[PubMed](#)]
55. Kitchamsetti, N.; Kim, D. A Facile Method for Synthesizing MOF Derived ZnCo<sub>2</sub>O<sub>4</sub> Particles on MXene Nanosheets as a Novel Anode Material for High Performance Hybrid Supercapacitors. *Electrochim. Acta* **2023**, *441*, 141824. [[CrossRef](#)]

**Disclaimer/Publisher's Note:** The statements, opinions and data contained in all publications are solely those of the individual author(s) and contributor(s) and not of MDPI and/or the editor(s). MDPI and/or the editor(s) disclaim responsibility for any injury to people or property resulting from any ideas, methods, instructions or products referred to in the content.